SUPPORTING INFORMATION FOR

Quantification and Healing of Defects in Atomically Thin Molybdenum Disulfide: Beyond Controlled Creation of Atomic Defects

Kazunori Fujisawa[*,†], *Bruno R. Carvalho*[*,†], *Tianyi Zhang, Néstor Perea-López, Zhong Lin, Victor Carozo, Sérgio L. L. M. Ramos, Ethan Kahn, Adam Bolotsky, He Liu, Ana Laura Elías, Mauricio Terrones*[,†]

* These authors contributed equally to this work
† Correspondence to: fujisawa@endomoribu.shinshu-u.ac.jp (K.F.),
brunorc@fisica.ufrn.br (B.R.C.), mut11@psu.edu (M.T.)

This Supporting Information includes:

- **Section S1: Noise level of Raman image**
- **Section S2: Raman spectrum dependence to different ion dose**
- **Section S3: Temperature-dependent Raman results of a defective MoS$_2$**
- **Section S4: Representative STEM-HAADF images**
- **Section S5: Polymer residue on MoS$_2$ membrane after Ga$^+$ irradiation**
- **Section S6: Finite crystal length analysis of pristine suspended MoS$_2$**
- **Section S7: Azimuthal representation of finite crystal length distribution**
- **Section S8: Finite crystal length analysis result of simulated STEM images**
- **Section S9: Fitting parameter for 1D finite crystal length distribution**
- **Section S10: Defect healing in suspended MoS$_2$ *via* H$_2$S annealing**
- Figure S1: **Raman image of the LA-band**
- Figure S2: **Raman spectrum evolution as a function of the ion dose effect**
- Figure S3: **Temperature-dependent Raman study for different ion doses**
- Figure S4: **High magnification STEM-HAADF image of pristine and defective MoS$_2$**
- Figure S5: **Low magnification STEM-HAADF image of pristine and defective MoS$_2$**
- Figure S6: **Polymer residue layer on MoS$_2$ revealed by STEM-HAADF**
- Figure S7: **Finite crystal length distribution in pristine MoS$_2$**
- Figure S8: **Azimuthal representation of finite crystal length distribution**
- Figure S9: **Finite crystal length analysis of simulated STEM-HAADF image of MoS$_2$**
- Figure S10: **The defect healing process on suspended MoS$_2$**
- Table S1. Fitting parameters for *k*-Gamma function used to fit 1D finite crystal length distribution

Section S1: Noise level of Raman image.

Figure S1 (a) and (b) shows the raw Raman image created by using the LA-band of MoS_2 spectra, and (b) intensity line profile of the Raman image, respectively. The high noise level of the Raman image is due to a relatively low signal of the LA-band of MoS_2. Similar intensity variation is observed in the substrate region without MoS_2.
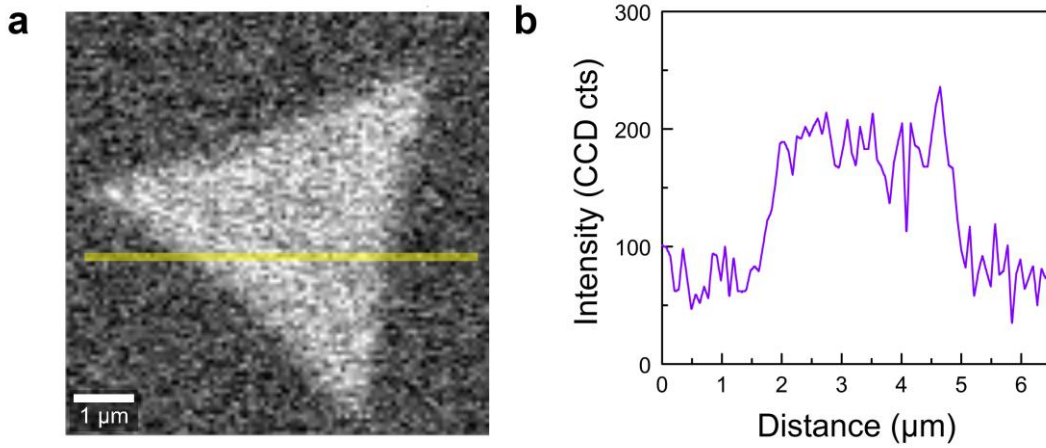

Figure S1: **Raman image of the LA-band.** (**a**) Raman LA-band image obtained using 2.33 eV, (**b**) obtained LA-band intensity line profile along the yellow line in (a).

Section S2: Raman spectrum dependence to different ion dose.

Figure S2 shows the Raman spectral evolution of monolayer MoS_2 bombarded with Ga^+, for different ion doses measured, at 2.41 eV and 2.54 eV laser energies. The bottom spectrum represents the pristine sample for comparison. Note that the spectrum evolves as the ion dosage increases. Notably, we can observe changes in position and linewidth for E' and A_1' modes, an indication that the sample starts to become amorphous. More specifically, for supported (suspended) MoS_2 triangles showed an obvious broadening of E' and A'_1 modes irradiated with $\eta_{ion} = 4.76 \times 10^{13}$ ions/cm^2 (6.40×10^{14} ions/cm^2), and further broadening and shift of E' and A'_1 modes are found at $\eta_{ion} = 1.00 \times 10^{14}$ ions/cm^2 (1.23×10^{14} ions/cm^2). Additionally, one can also observe how the defective Raman features vary with increasing defect density. Once again, we notice that the defective Raman peaks are more pronounced at 2.41 eV when compared to 2.54 eV. This can be attributed to the density of states of the material.
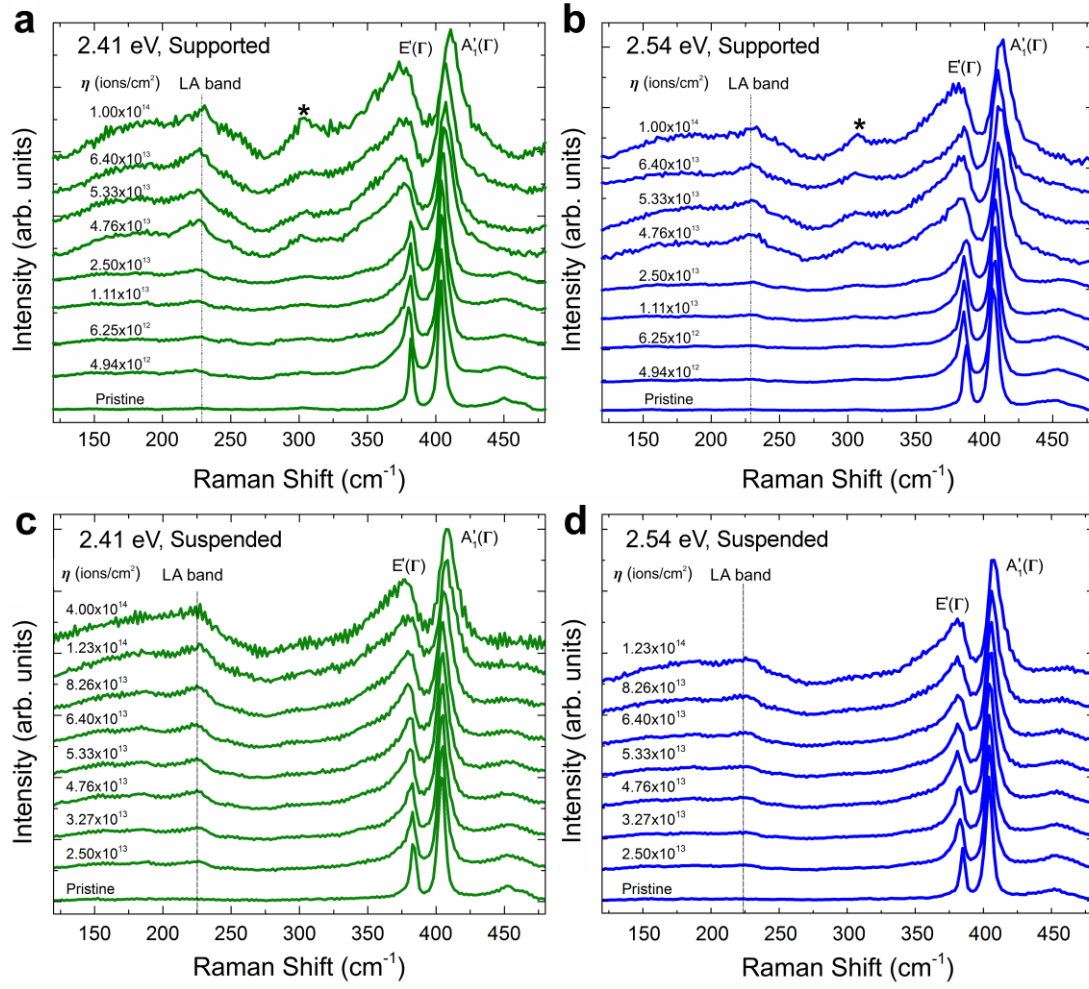
Figure S2: **Raman spectrum evolution as a function of the ion dose effect.** Raman spectra of defective MoS_2 on silicon substrate for different amounts of ion dose measured for (**a**) 2.41 eV and (**b**) 2.54 eV laser excitation energies, respectively. The asterisk (*) represents the 2TA(**X**) Si peak. Raman spectrum of a suspended MoS_2 collected at (**c**) 2.41 eV and (**d**) 2.54 eV laser excitation energies.

Section S3: Temperature-dependent Raman results of a defective MoS₂.

Figure S3 shows the temperature-dependent Raman spectrum measured at 2.54 eV laser energy for three different ion dosages: 2.50×10^{13}, 4.76×10^{13}, and 1.00×10^{14} ions/cm^2, respectively. The Raman spectra were collected at vacuum conditions in a 20–280 K temperature range. Notice that as the temperature decreases the defective LA-band intensity increases.
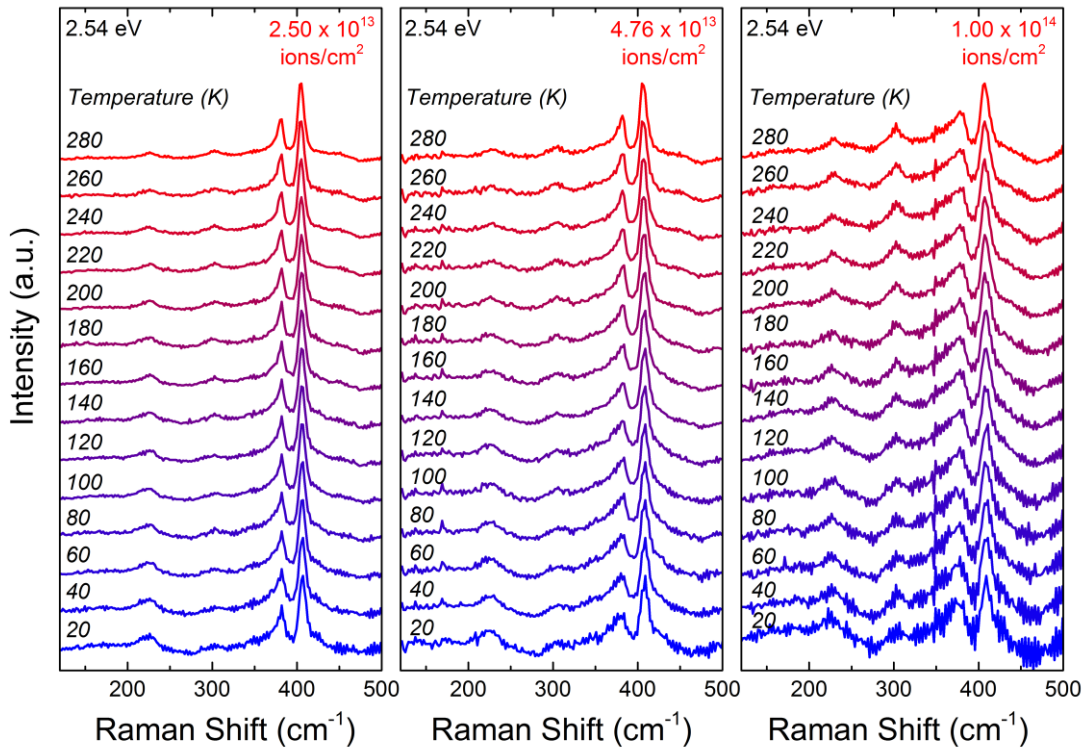

Figure S3: **Temperature-dependent Raman study for different ion doses.** Temperature-dependent Raman results of defective MoS₂ for three different amounts of ion dose: 2.50×10^{13}, 4.76×10^{13}, and 1.00×10^{14} ions/cm^2. The spectra were collected at 2.54 eV and normalize by the A'_1 peak for better visualization.

Section S4: Representative STEM-HAADF images.

Figure S4 and **S5** show STEM-HAADF image of pristine and irradiated MoS_2 at high magnification and low magnification, respectively. Even in the pristine MoS_2 sample, some monosulfur vacancies (V_S) are present. The size of the defect increases as increasing the irradiation dose. Low magnification STEM-HAADF images are used for the statistical analysis (**Figure 3**) and the finite crystal length analysis (**Figure 4**).
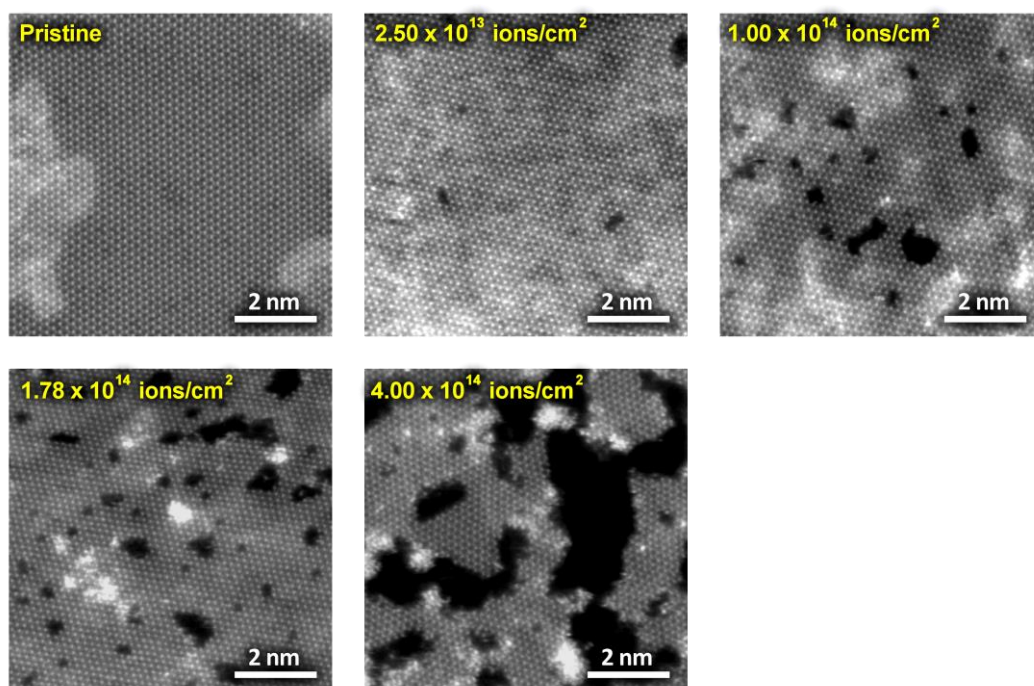

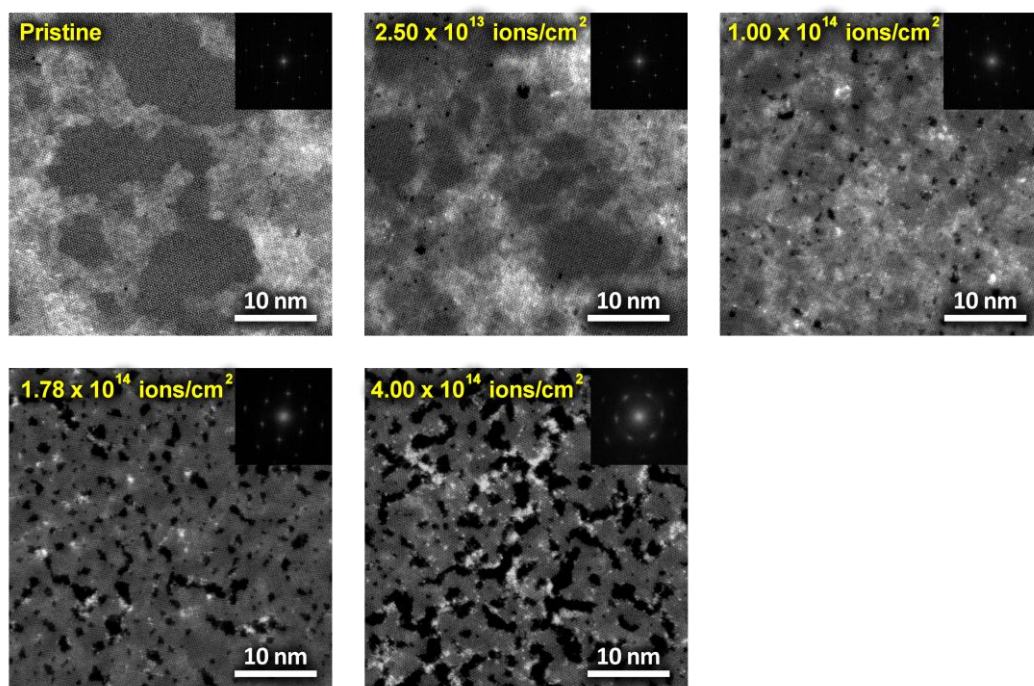Figure S4: **High magnification STEM-HAADF image of pristine and defective MoS₂.**

Figure S5: **Low magnification STEM-HAADF image of pristine and defective MoS₂.**
The insets correspond to the fast Fourier transform (FFT) patterns for each image.

Section S5: Polymer residue on MoS$_2$ membrane after Ga$^+$ irradiation.

Since the PMMA-assisted wet-chemical substrate etching method was used to transfer MoS$_2$ monolayer grown on SiO$_2$/Si substrate, there is some PMMA polymer residue layer on the surface of MoS$_2$. **Figure S6** shows the remaining polymer residue layer on the MoS$_2$ surface (highlighted by yellow-color, **Figure S6 (a)**). At the highest dose we used, the polymer residue layer was completely removed (**Figure S6 (b)**).
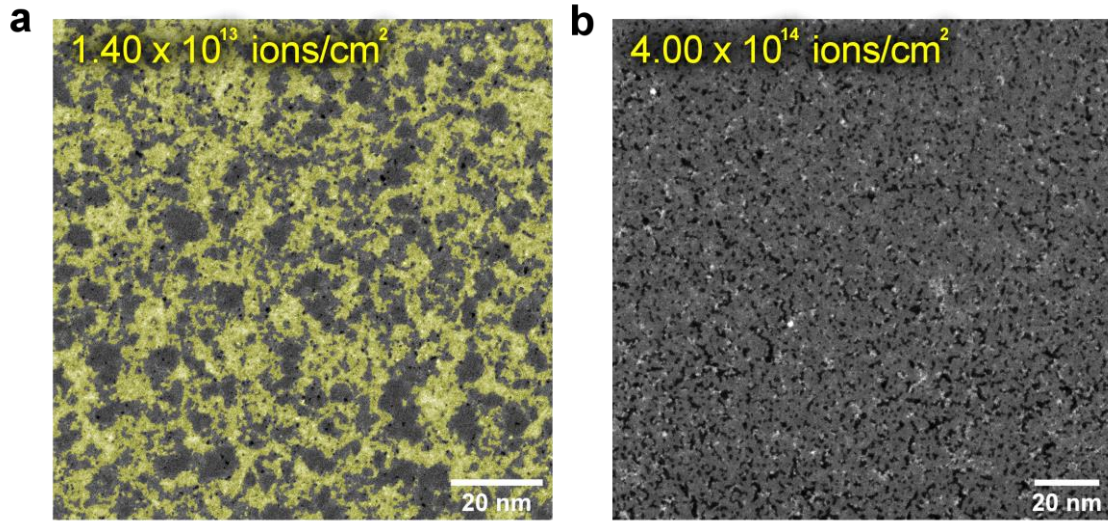

Figure S6: **Polymer residue layer on MoS$_2$ revealed by STEM-HAADF.** Defective MoS$_2$ irradiated with (**a**) 1.40×10^{13} (**b**) and 4.00×10^{14} ions/cm^2. The polymer residue layers are highlighted by yellow color.

Section S6: Finite crystal length analysis of pristine suspended MoS$_2$.

Figure S7 shows finite crystal length distribution in pristine MoS$_2$. Since there is no obvious defect besides monosulfur vacancies (V$_S$), there is no obvious feature in the finite crystal length distribution.
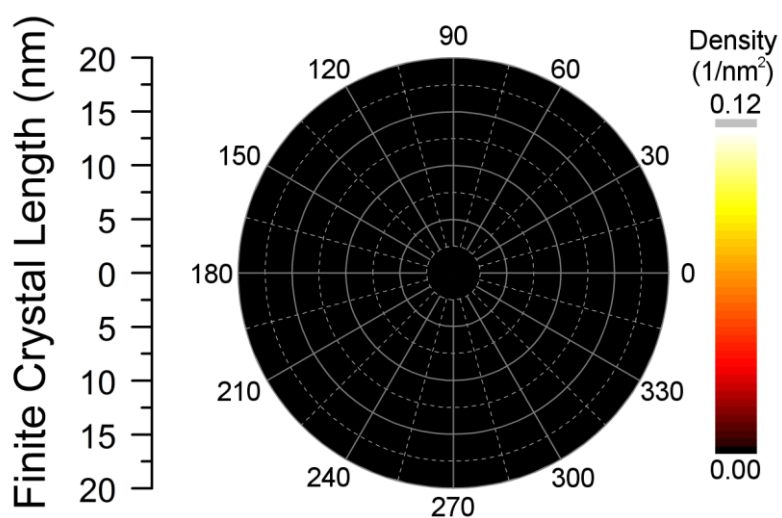

Figure S7: **Finite crystal length distribution in pristine MoS$_2$.** Acquired finite crystal length distribution from pristine MoS$_2$. There is no obvious feature in the distribution.

Section S7: Azimuthal representation of finite crystal length distribution.

Figure S8 shows the distribution of finite crystal length in pristine and irradiated MoS_2. **Figure S8** is intrinsically the same as radial representation (**Figure 3a**) in the main text. The finite crystal length shows the uniform distribution across the whole image analysis direction which indicates that the defects are introduced to MoS_2 isotropically.
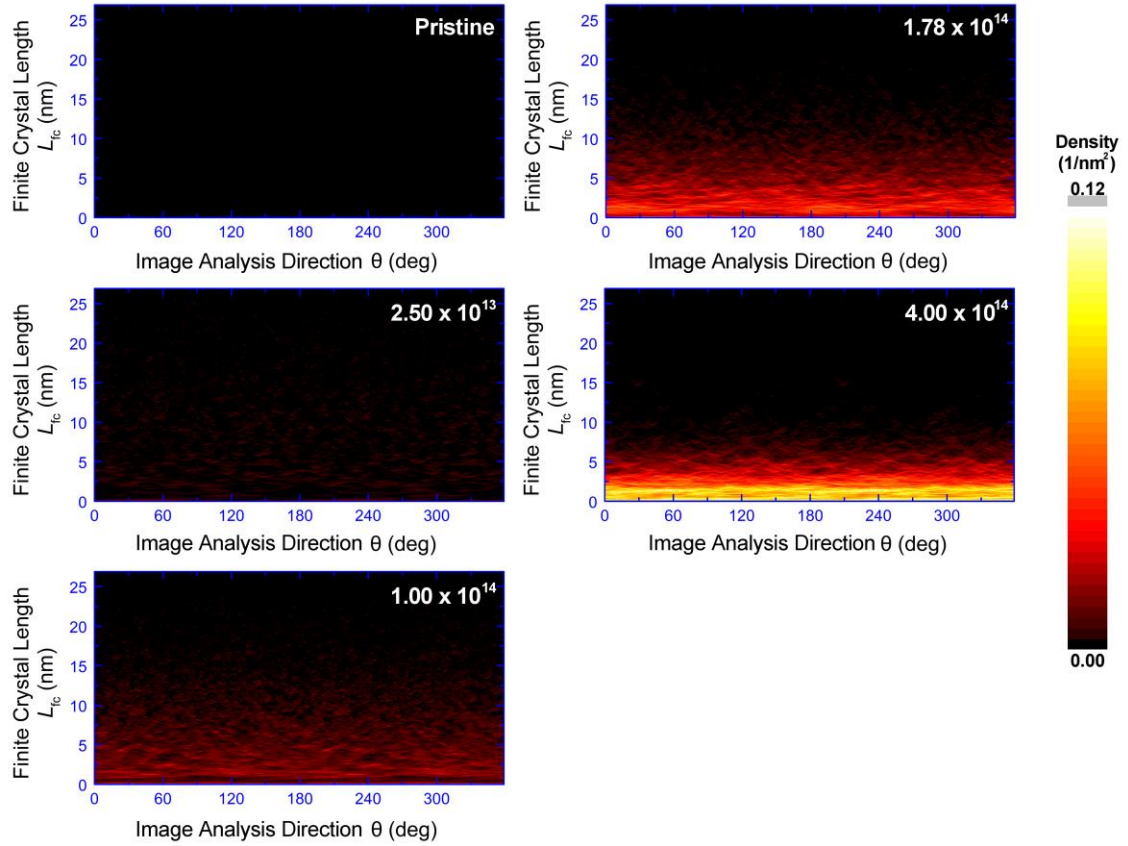

Figure S8: **Azimuthal representation of finite crystal length distribution.** The histograms of finite crystal length for each image analysis direction θ. The color code represents the density of finite crystal length.

Section S8: Finite crystal length analysis result of simulated STEM images.

Figure S9 shows the simulated STEM-HAADF images (a, d and g), the image analysis direction (θ) dependent finite crystal length distribution (b, e, and h), and the integrated 1D finite crystal length distribution (c, f, and i) obtained from the monolayer MoS_2 crystals with periodic MoS_6 defect, line defect, and random MoS_6 defect, respectively. The large simulated STEM-HAADF images as experimental STEM-HAADF image (38.4×38.4 nm) were created by tiling small ones periodically and randomly. Different features are showing up in the 2D (**Fig. S9 b, e, and h**) and 1D (**Fig. S9 g, h and i**) finite crystal length distribution depending on the periodicity and anisotropicity of the defects.
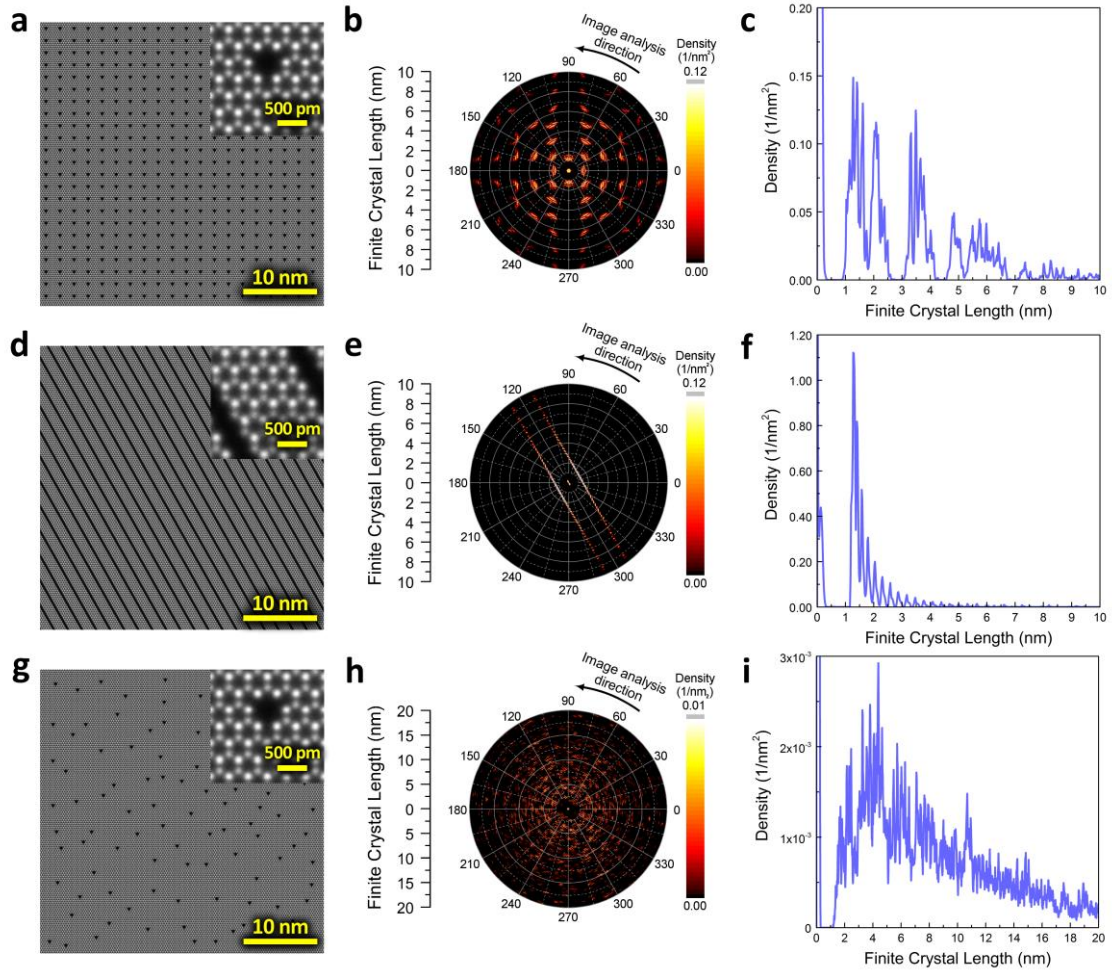

Figure S9: **Finite crystal length analysis of simulated STEM-HAADF image of MoS₂.** Simulated STEM-HAADF image of (**a**) periodic MoS_6 defects, (**d**) line defect, and (**g**) random MoS_6 defects, and corresponding 2D finite crystal length distribution (**b**, **e**, **h**), and 1D finite crystal length distribution (**c**, **f**, **i**), respectively.

Section S9: Fitting parameter for 1D finite crystal length distribution.

Table S1 describes the used parameter for the fitting of 1D finite crystal length distribution (**Figure 4c**). The mean finite crystal length L_{fc} decreased as the ion dose used for irradiation increases. An indicator of heterogeneity k slightly increased as the ion dose increases.

Table S1. Fitting parameters for k-Gamma function
used to fit 1D finite crystal length distribution.

Ion Dose *(ions/cm²)*	Fitting Parameter	
	Mean finite crystal length L_{fc} (nm)	Heterogeneity k
2.50×10¹³	8.37	1.27
3.27×10¹³	7.95	1.35
4.76×10¹³	5.99	1.38
5.33×10¹³	6.13	1.24
6.40×10¹³	5.11	1.39
8.26×10¹³	4.40	1.47
1.00×10¹⁴	5.58	1.37
1.23×10¹⁴	3.92	1.61
1.78×10¹⁴	3.51	1.57
2.78×10¹⁴	3.55	1.47
4.00×10¹⁴	2.34	1.71

Section S10: Defect healing in suspended MoS$_2$ *via* H$_2$S annealing.

Figure S10 shows Raman and photoluminescence spectroscopic results of suspended pristine, ion irradiated and H$_2$S annealed MoS$_2$. A pristine MoS$_2$ crystal was transferred onto a Si TEM chip with a holey SiN$_X$ membrane. The Raman and photoluminescence signals were collected from the suspended MoS$_2$ region at the center of the SiN$_X$ hole. The healing behavior is also observed after H$_2$S annealing in suspended MoS$_2$ condition, more specifically LA-band in Raman spectrum decreased and photoluminescence signal was partially recovered.
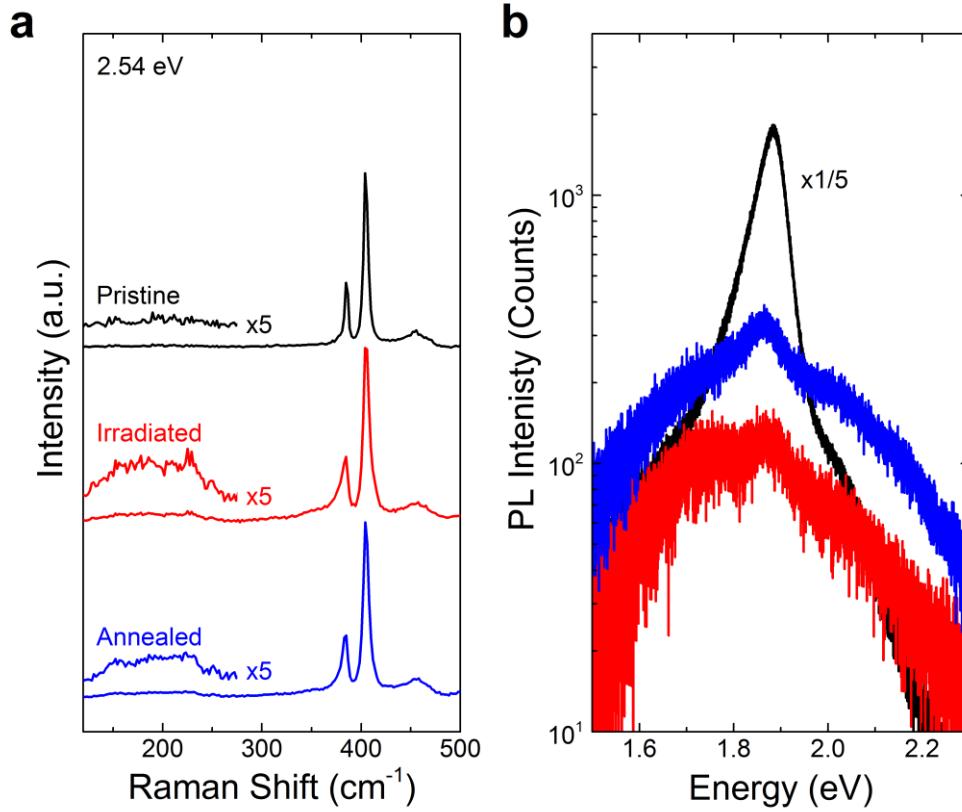

Figure S10: **The defect healing process on suspended MoS$_2$.** (**a**) Raman and (**b**) photoluminescence spectra of pristine (black), ion irradiated (red), and H$_2$S annealed (blue) MoS$_2$ measured at 2.54 eV laser excitation energy. All measurements and treatment, such as Ga$^+$ ion irradiation and H$_2$S annealing, were carried out on the suspended condition.